Journal of Microelectronics and Electronic Packaging (2016) **13**, 58-63

ISSN: 1551-4897

A New In-Line Laser-Based Acoustic Technique for Pillar Bump Metrology

Todd W. Murray,[1,*] Andrew Bakir,[1] David M. Stobbe,[1] Michael J. Kotelyanskii,[2] Robin A. Mair,[2] Manjusha Mehendale,[2] Xueping Ru,[2] Jonathan D. Cohen,[2] Michelle T. Schulberg,[3] Priya Mukundhan,[2] and Timothy J. Kryman[2]

***Abstract*—The drive to reduce the interconnect pitch and increase the number of connections for packaging in mobile devices has led to the development of copper pillar bumps. The key drivers for the adoption of copper pillars are improved performance, reduced form factor, and lower cost. In this article, we present a laser-based acoustic technique for the characterization of multilayer pillars. This noncontact technique has a high sensitivity for materials characterization with micron-scale spatial resolution. Absorption of laser light causes excitation of elastic waves that propagate through the pillar and are reflected by the pillar walls, exciting vibrational modes in the structure. We have demonstrated that our approach is sensitive to the thicknesses of individual layers in bilayer and trilayer copper pillar stacks. Focused ion beam scanning electron microscopy (FIB-SEM) has been used to optimize the model and to validate the accuracy of the technique.**

***Keywords*—Copper pillar bump stacks, acoustic metrology, advanced packaging**

Introduction

Bump interconnect technology plays a critical role in three-dimensional integration of semiconductor devices, and is a key enabler of cost effective middle-end supply chain processes. Copper pillar technology offers excellent electromigration performance for high-current carrying applications resulting in superior reliability of the end products. Fine-pitch copper pillar bumps have replaced conventional solder bumps in high-end processors, graphics, field-programmable gate arrays, power amplifiers, handheld consumer electronic devices, as well as servers and network applications [1-3].

Copper pillar bumps are manufactured with the same materials and processing techniques as conventional solder bumps. The bump base is defined by lithographic patterning of a layer of photoresist, and the bump metal stacks are electroplated in the open features on top of an under bump metal (UBM). The photoresist is subsequently stripped, and any UBM not protected by the bump is etched away. The wafer then goes through reflow and cleaning processes. Typical bump metal stacks are bilayer Cu/SnAg and trilayer Cu/Ni/SnAg.

Careful monitoring and control of the copper pillar's critical features and physical properties are essential to ensuring a high-quality, reliable bump structure. Several noncontact methods exist for measurements of step heights and coplanarity, e.g., confocal sensors, triangulation sensors, and scanning white light interferometry, but these technologies do not provide individual layer thickness in a multilayer pillar stack. Instead, any deviation in the coplanarity of the bumps is evaluated using destructive and time-intensive off-line techniques such as focused ion beam (FIB) milling and scanning electron microscopy (SEM). There is a need in the industry for a nondestructive in-line metrology tool that can provide feedback on pillar bump coplanarity and layer thicknesses. In this article, we describe a laser-based acoustic system for determining the thickness of individual layers in copper pillar stacks. The technique has shown the ability to measure thicknesses both before and after the photoresist strip.

Measurement Theory and Methodology

Laser-based ultrasonics has been proved to be an effective tool for a variety of materials characterization applications, ranging from thickness and elastic property measurements of thin films and coatings [4-7] to the characterization of micro and nanomechanical systems [8, 9], to defect detection in large scale graphite epoxy composite inspection [10]. Laser ultrasonics (LU) uses pulsed or modulated continuous wave lasers to excite high-frequency ultrasound in a test object through thermoelastic expansion. The displacement at the sample surface is detected with a second optical probe, typically using interferometry, optical beam deflection, or ultrasound-induced changes in surface reflectivity [11]. As opposed to conventional acoustic microscopy, LU does not require a coupling medium, and is completely a noncontact technique. In addition, the generation and detection lasers can be tightly focused on the sample surface, offering excellent spatial resolution and allowing inspection of small-scale structural features. The frequency content of laser-generated ultrasound is dependent on the pulse width and spatial distribution of the laser energy on the sample surface, as well as the optical properties of the

The manuscript was received on January 7, 2016; revision received on April 1, 2016; accepted on April 1, 2016

The original version of this paper was presented at IMAPS 48th International Symposium on Microelectronics (IMAPS' 2015), October 26-29, 2015, Orlando, FL.

[1]Department of Mechanical Engineering, University of Colorado, Boulder, Colorado 80309

[2]Rudolph Technologies, 550 Clark Drive, Budd Lake, New Jersey 07828

[3]TEL NEXX, Inc., 900 Middlesex Turnpike, Building 6, Billerica, Massachusetts 01821

*Corresponding author; email: todd.murray@colorado.edu

doi:10.4071/imaps.501

sample. Microchip lasers with a pulse width on the order of a nanosecond can, e.g., generate ultrasound frequencies in the range of hundreds of megahertz.

To measure pillar bumps, we irradiate the top surface of the pillar using a pulsed laser source. Optical absorption leads to heating of the pillar surface and subsequent thermoelastic expansion, producing ultrasound waves that propagate through the structure and couple into resonant vibrational modes. The temporal evolution of these vibrations is tracked by measuring the normal displacement on the sample surface over time using an optical interferometer. The detected signal is postprocessed using a Fourier transform to determine the vibrational mode frequencies. These frequencies are sensitive to the pillar geometry (diameter and layer thicknesses) and the mechanical properties of the layers.

To relate the measured vibrational mode frequencies to pillar parameters, a numerical model has been developed using explicit time domain finite element modeling (FEM) with the PZFlex code (Weidlinger Associates, Mountain View, CA). As an example, consider the trilayer pillar shown in Fig. 1. Here, the pillar is 60 μm in diameter with copper (29.11 μm), Ni (2.18 μm), and SnAg (16.63 μm) layers on a base material composed of TiW (140 nm), polyimide (4.37 μm), and silicon (semi-infinite substrate). All materials are modeled as isotropic, and the longitudinal (V_L) and shear (V_S) wave velocities and densities of these materials are given in Table I. Most of the material properties were taken from the literature [12], with the exception of copper and polyimide. Both Cu and polyimide have a range of reported properties depending on, e.g., processing conditions or texture. The values reported in Table I were found to give the best agreement between experiment and simulation on pillars of known geometry.

Absorption of laser light at the pillar surface produces rapid heating followed by slow cooling through thermal diffusion. The cooling process is slow compared to the time scale of the pillar vibrations, and is therefore neglected. The heating process is modeled by a surface force dipole, with a time dependence given by the integral of the 3.0 ns Gaussian temporal heating pulse. This simulates the accumulation of heat as light is absorbed at the sample surface. We used a two-dimensional model with cylindrical symmetry, with the laser generation source (12 μm spot size with a Gaussian distribution) centered on the top of the pillar. The surface dipole in this case is a shear force acting at the top of the pillar, and directed away from the pillar center, with the magnitude of the force proportional to the derivative of the intensity distribution. The pillar and upper substrate surface are traction free, and the sides and bottom of the substrate have absorbing boundary conditions. Further details regarding laser excitation of ultrasound can be found in the literature [13, 14].

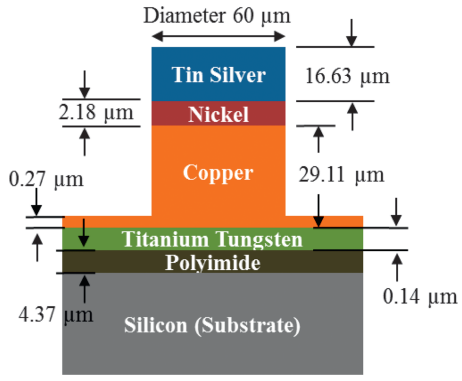

Fig. 1. Geometry and materials in trilayer pillar.

Table I
Material Properties Used in the Simulation

Material	V_L (m/s)	V_S (m/s)	Density (kg/m^3)
Tin silver	3,469	1,622	7,360
Nickel	5,814	3,078	8,907
Copper	4,960	2,509	8,933
Titanium tungsten	5,266	2,906	18,770
Polyimide	2,423	627	1,325
Silicon	8,417	5,846	2,329

The normal displacement at the center of the pillar is output as a function of time after excitation. The result is shown in Fig. 2a, where the signal is seen to oscillate and slowly

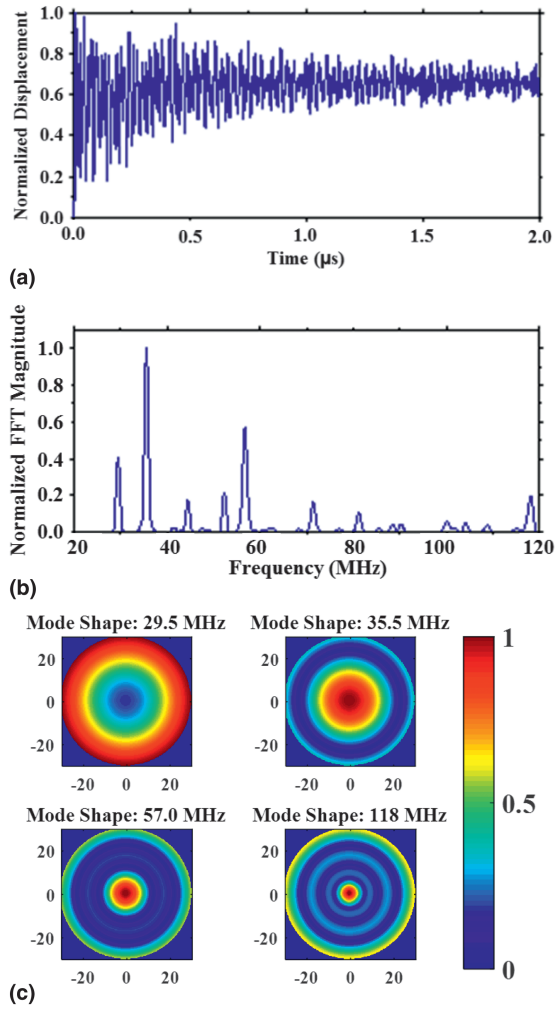

Fig. 2. (a) Normal displacement of the pillar surface calculated at the center of the pillar, (b) spectrum of normal displacement measured on epicenter, and (c) magnitude of the displacement over the top surface of the pillar showing the mode shapes.

decay in time. The vibration mode frequencies are identified through a Fourier transform of the time domain data, and the result is shown in Fig. 2b. A large number of peaks, each corresponding to a different vibrational mode, are seen in the figure. In Fig. 2c, the magnitude of the normal displacement at the pillar surface is plotted for modes identified at 29.5, 35.5, 57.0, and 118 MHz. As expected, the higher frequency modes show more complex structure and rapid variation over the sample surface. The rich spectral content of the signal offers an attractive means of characterizing a given pillar structure, and forms the basis of our pillar bump metrology approach.

This technique requires complete information on the stack, including mechanical properties of all the layers to develop the model. As a result, mapping out this space and setting up recipes can become complicated and time consuming. To make the method more suitable for a high-volume manufacturing (HVM) environment, we have also explored using FEM simulations to derive the characteristic frequency dependence of layer thickness and bump diameters. A multidimensional interpolation is performed on the lookup table derived from the FEM to find the best solution.

Experimental Setup

A basic schematic of the experimental setup is shown in Fig. 3. A pulsed and frequency-doubled Nd:YAG laser operating at a wavelength of 532 nm is used for ultrasound generation. The pulse width is approximately 300 ps. The generation laser reflects from a mirror on a gimbal mount, travels through a relay lens system, and on to the pillar surface through a long working distance objective. The optical system allows precise positioning of the laser spot within the field of view of the objective, as well as control over the generation spot size. A Michelson interferometer with a continuous wave laser operating at a wavelength of 660 nm detects the displacement of the pillar surface following laser excitation. The laser output is directed to a beam splitter where it is divided into signal and reference beams. The reference beam reflects off an actively stabilized mirror, and is sent to a photodiode with a 1-GHz bandwidth. The signal beam is directed through the long working distance objective to the pillar surface, and the reflected light is collected and returned to the photodetector. The output from the photodetector is digitized and processed by a computer. For the results presented here, the generation and detection lasers overlap and are positioned near the center of the pillar. However, we have noted that the system has the flexibility to position these beams independently at any point on the surface. The excitation laser spot size is approximately 30 μm in diameter while the detection spot size is approximately 3 μm in diameter. At the sample surface, the detection laser power was 30 mW, and the generation laser energy was approximately 0.05 μJ per pulse. The surface temperature rise was not quantified. The total laser power was selected such that we were operating in the thermoelastic regimen, and thus avoiding thermally induced damage to the pillar surface.

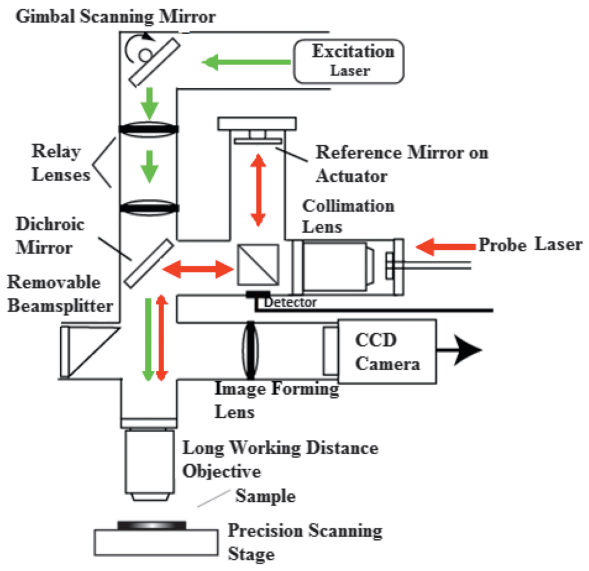

Fig. 3. Schematic representation of the optical setup.

Bilayer and trilayer pillars of Cu (30 μm ± 10%)/Ni (0-4 μm)/SnAg (15 μm ± 10%) with diameters ranging from 50 to 140 μm were deposited on a TEL NEXX Stratus S300 electroplating tool. Selected pillars on each wafer were measured on a Zygo Series 6000 interferometric profilometer, which measures the height of the pillar compared with the surrounding area. The features were measured before deposition to give the photoresist thicknesses and after electroplating each individual layer. Finally, the total height of the stack was measured again after stripping the photoresist. To develop a model and also to validate the accuracy of our measurements, selected samples were cross-sectioned using FIB-SEM.

Results

We evaluated two different modeling approaches to measure the layer thicknesses of the pillar structures: a model-based inversion approach and a lookup table approach.

A. Model-Based Inversion

Time domain experimental data are collected and Fourier transformed to determine the spectral response. The frequencies of several strong vibrational modes are identified and compared with the peak frequencies calculated using the finite element model for a given set of layer thicknesses. The layer thicknesses are then changed, and the comparison is repeated. The predicted layer thicknesses are taken as those that minimize the sum of the squared error ϕ between the calculated and known peak frequencies:

$$\phi = \sum_{i=1}^{N} \left(f_i^{\mathrm{M}} - f_i^{\mathrm{C}} \right)^2 \tag{1}$$

where f_i^{M} and f_i^{C} are the measured and calculated frequencies of mode i, and N is the total number of modes selected. In addition to layer thicknesses, the spectral response is also dependent upon elastic properties of all materials, represented by V_{L}, V_{S}, and density. Since the properties of polyimide and Cu can vary with processing conditions, we determined their values for these samples using the same minimization approach described in eq. (1), but using pillars with "known geometries" measured with FIB-SEM. Once the properties of

the copper and the polyimide were determined, they were fixed, leaving only the layer thicknesses and the pillar diameter as unknowns. The thickness of the polyimide and TiW layers for all samples were held constant in the modeling, as small differences in these values observed through microscopy had minimal influence on the spectral response. Fig. 4a shows a comparison between the measured spectrum and the best-fit spectrum for a bilayer Cu/Ni pillar with a diameter of 60 μm. This structure is an intermediate step in the formation of a trilayer Cu/Ni/SnAg pillar stack. The best fit (found using $N = 3$ peaks near 37, 42, and 82 MHz) gave a Cu thickness of 32.8 μm and a Ni thickness of 2.0 μm, which can be compared with the FIB-SEM measurement of 32.54 μm and 2.15 μm for Cu and Ni, respectively. Fig. 4b shows the sum of the squared errors (ϕ) for different combinations of Cu and Ni heights, or error surface.

The fit between theory and experiment is excellent, with the minimum error below 0.1 MHz. Comparison between LU measurements and FIB-SEM on other pillars also provided consistent results.

Trilayer Cu/Ni/SnAg pillars present additional challenges in extracting the thickness of all three layers. The spectrum is significantly more complex, with many more modes generated than in the two layer case. Fig. 5 shows the measured spectrum on the same pillar as Fig. 4a but after deposition of a 15.76-μm layer of SnAg. Also shown in Fig. 5 is the best-fit spectrum

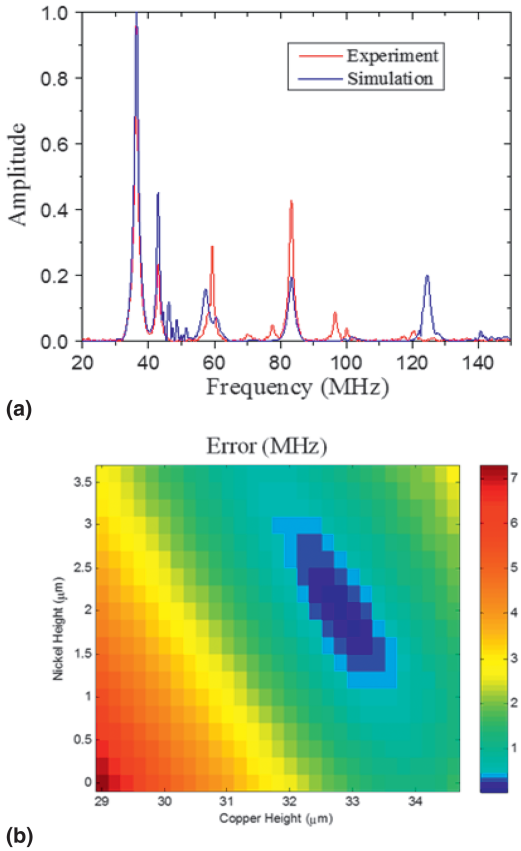

Fig. 4. (a) A comparison of the measured and calculated response for a Cu (32.8 μm)/Ni (2.0 μm) pillar. (b) The error (ϕ) between measurement and calculation for a range of Cu and Ni heights. The error is minimized at Cu/Ni heights of 32.8/2.0 μm.

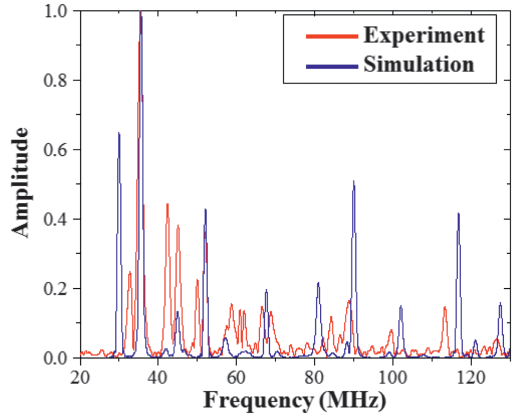

Fig. 5. The best-fit calculated response for a Cu/Ni/SnAg pillar with layer thicknesses of 33.4/1.8/15.2 μm, and the measured response of a pillar with layer thicknesses of 32.54/2.15/15.76 μm as determined through FIB/SEM.

from the simulation. Here, we have assumed that the total pillar height (50.45 μm) is known, leaving two unknowns in the determination of the three layer thicknesses. In practice, the total pillar height could be found using complementary optical approaches incorporated into our system. The agreement between simulation and experiment for the trilayer is not as strong as for the bilayer case. However, several of the peaks in the simulation result line up nicely with the measured peaks, including the strongest peak ∼36 MHz, the peak at 45 MHz, and a third strong peak at 52 MHz. Other peaks, such as that predicted by the simulation at 30 MHz, are not observed in the experimental results. The reason for this is not clear, but may stem from the positioning of the source and receiver on the sample. We modeled excitation and detection at the exact center of the pillar, but the source and receiver positions were not precisely controlled during the experiments. Altering the forcing function on the sample surface can lead to different amounts of energy being coupled into each mode. Nevertheless, using the peaks that appear to be coincident, the simulation predicted Cu/Ni/SnAg thicknesses of 33.4/1.8/15.2 μm while the FIB-SEM measurements gave thicknesses of 32.54/

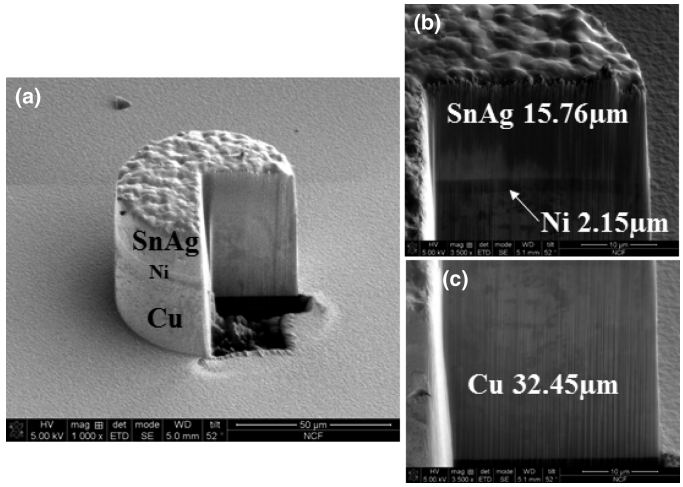

Fig. 6. FIB-SEM cross section of (a) trilayer copper pillar stack and zoom-in of (b) Ni and SnAg layers and (c) Cu layer.

2.15/15.76 μm (Fig. 6). One of the key challenges in determining the three thicknesses in a trilayer pillar is the similar properties of Cu and Ni, which makes it difficult to distinguish the contributions of these two materials using only lower frequency modes. However, higher frequency modes (>100 MHz) are very sensitive to changes in the Cu and Ni layer thicknesses and may provide a solution, allowing for all three thicknesses to be found in a reliable manner. We noted that the SnAg surface exhibits some degree of roughness. FEM simulations showed that mild surface roughness, with a root-mean square value on the order of 0.5 μm, has little impact on the vibrational spectra.

B. Lookup Table Approach

For the simpler Cu/SnAg bilayers, we also evaluated the validity of a lookup table-based approach for use in HVM. Vibrational modes that show strong correlation with the pillar properties were identified from the FEM simulations to be ~20, 46 and 80 MHz for a range of diameters and thickness (T_{Cu} and T_{SnAg}). Time domain measurement signals acquired before photoresist strip (Fig. 7a) were analyzed using Fourier transformation in two different time windows. Peaks of interest are identified in Figs. 7b and 7c. Copper and SnAg thickness are simultaneously reported (Fig. 8) following a multidimensional interpolation. The measurement sites are randomly selected to represent different target thicknesses (shown in Fig. 8) of both layers. One can readily see the contributions from the individual layers to the total thickness. Also shown in this figure for comparison is the total (Cu + SnAg) thickness obtained from Zygo optical inspection tool.

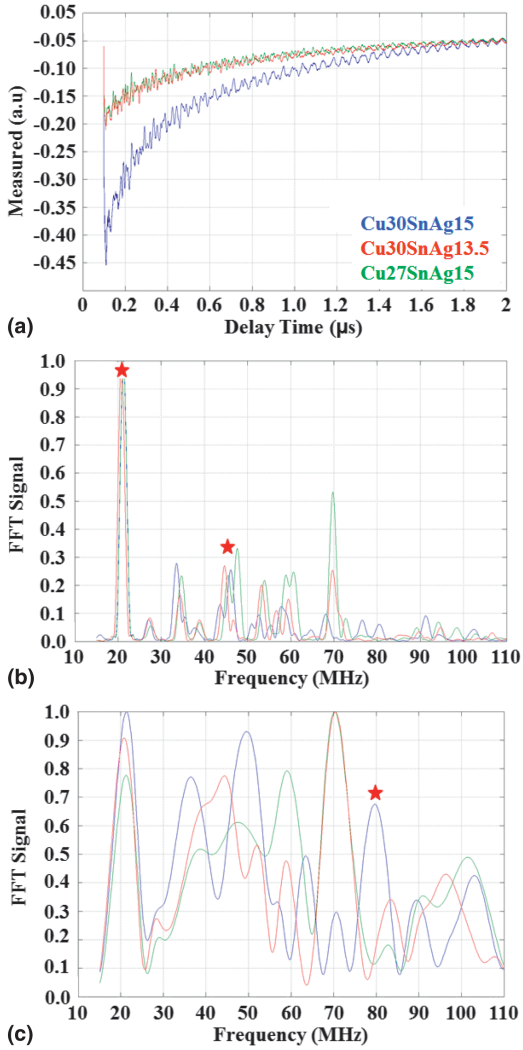

Fig. 7. (a) Measurement signal from Cu/SnAg bilayers, (b) and (c) Fourier transform of signals in two different time ranges.

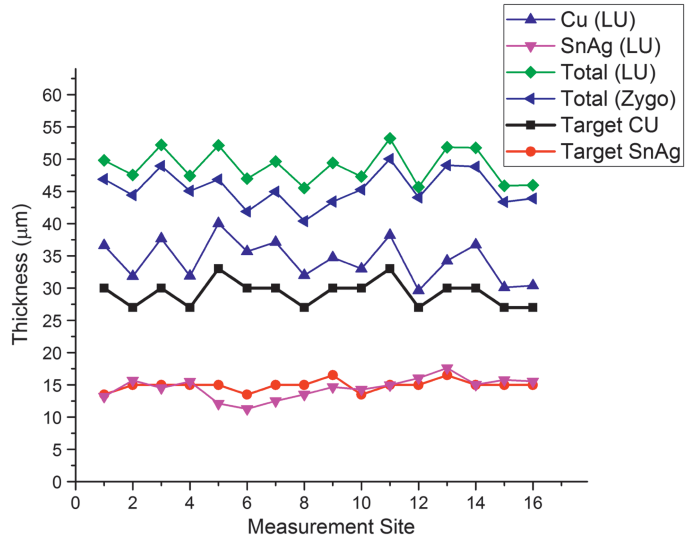

Fig. 8. Cu/SnAg profiles across 16 measurement sites. LU simultaneously reports Cu and SnAg thicknesses. The target thickness for Cu and SnAg is also provided. A comparison of total thickness between LU and Zygo shows very good agreement.

In general, we see very good correlation between the two techniques (R^2 ~0.9). Some of the variations observed in the profiles are attributed to wafer placement differences between the systems. It is noteworthy to point out that the acoustic measurement can be made before photoresist strip and can be used for assessing the whole stack without the need to interrupt the plating process.

Conclusions

LU is a promising technique for in-line copper pillar bump metrology. We have demonstrated that this noncontact, nondestructive technique is uniquely capable of measuring individual layer thickness in Cu/SnAg and Cu/Ni/SnAg pillars before photoresist removal. The small spot size capability and fast measurement times (<10 s per site) make it attractive for in-line monitoring, especially on fine-pitch bumps. The technique can be used to provide feedback on plating processes during development and as a failure analysis tool in a manufacturing environment to detect excursions that impact the coplanarity of the bumps. Additional improvements to robustly distinguish between Cu and Ni contributions to a trilayer stack are underway.

Acknowledgment

TEL NEXX gratefully acknowledges the contributions of co-op students Noah Luszcz, Victor Antontsev, Jordan Green,

Joe Niemiroski, and Sean Barrows in depositing and measuring the copper pillar test wafers.

References

[1] P. Garrou, M. Koyanagi, and P. Ramm, *Handbook of 3D Integration: 3D Process Technology*, vol. 3, John Wiley & Sons, Weinheim, Germany, 2014.

[2] B.C. Wells, "Chip-scale packaging: processing, solutions and outlook," *3D Packaging*, November, pp. 36-38, 2012.

[3] D.S. Patterson, "2.5/3D packaging enablement through copper pillar technology," *Chip Scale Review*, Vol. 16, pp. 20-26, 2012.

[4] C. Thomsen, H.T. Grahn, H.J. Maris, and J. Tauc, "Surface generation and detection of phonons by picosecond light pulses," *Physical Review B: Condensed Matter and Materials Physics*, Vol. 34, pp. 4129-4138, 1986.

[5] T.W. Murray, S. Krishnaswamy, and J.D. Achenbach, "Laser generation of ultrasound in films and coatings," *Applied Physics Letters*, Vol. 74, No. 23, pp. 3561-3563, 1999.

[6] D. Schneider and M.D. Tucker, "Non-destructive characterization and evaluation of thin films by laser induced ultrasonic surface waves," *Thin Solid Films*, Vol. 290-291, pp. 305-311, 1996.

[7] C. Hernandez, T.W. Murray, and S. Krishnaswamy, "Photo-acoustic characterization of the mechanical properties of thin films," *Applied Physics Letters*, Vol. 80, No. 4, pp. 691-693, 2002.

[8] B. Ilic, S. Krylov, K. Aubin, R. Reichenbach, and H.G. Craighead, "Optical excitation of nanoelectromechanical oscillators," *Applied Physics Letters*, Vol. 86, p. 193114, 2005.

[9] A. Sampathkumar, K.L. Ekinci, and T.W. Murray, "Multiplexed optical operation of distributed nanoelectromechanical systems," *Nano Letters*, Vol. 11, No. 3, pp. 1014-1019, 2011.

[10] J.-P. Monchalin, C. Neron, J.F. Bussiere, P. Bouchard, C. Padioleau, R. Héon, M. Choquet, J.-D. Aussel, C. Carnois, P. Roy, G. Durou, and J.A. Nilson, "Laser-ultrasonics: from the laboratory to the shop floor," *Advanced Performance Materials*, Vol. 5, pp. 7-26, 1998.

[11] R.J. Dewhurst and Q. Shan, "Optical remote measurement of ultrasound," *Measurement Science and Technology*, Vol. 10, pp. R139-R168, 1999.

[12] A. Briggs, *Acoustic Microscopy*, Clarendon, Oxford, UK, 1992.

[13] I. Arias and J.D. Achenbach, "Thermoelastic generation of ultrasound by line-focused laser irradiation," *International Journal of Solids and Structures*, Vol. 40, No. 25, pp. 6917-6935, 2003.

[14] S.J. Davis, C. Edwards, G.S. Taylor, and S.B. Palmer, "Laser-generated ultrasound: its properties, mechanisms, and multifarious applications," *Journal of Physics D: Applied Physics*, Vol. 26, pp. 329-348, 1993.